# Frequency-Dependent Complex Conductivities and Dielectric Responses of Indium Tin Oxide Thin Films from the Visible to the Far-Infrared

Ching-Wei Chen, Yen-Cheng Lin, Chia-Hua Chang, Peichen Yu, *Member, IEEE*, Jia-Min Shieh, and Ci-Ling Pan, *Senior Member, IEEE*

***Abstract*— Transparent and conducting indium tin oxide (ITO) thin films form an integral part for various optoelectronic devices. In this paper, we report the frequency-dependent complex conductivities and dielectric responses of several sputtered ITO thin films with thicknesses in the range of 189–962 nm by using terahertz time domain spectroscopy (THz-TDS), optical reflectance spectroscopy, and electrical measurements. The plasma frequencies are verified to be from 1590 to 1930 rad·THz, while the scattering times are in the range 6–7 fs based on the Drude free-electron model. The mobilities of the above ITO thin films are calculated to be 32.7–34.2 $cm^2\ V^{-1}\ s^{-1}$, whereas the carrier concentrations lie in the range 2.79–4.10 × $10^{20}\ cm^{-3}$. The electrical properties derived from the THz-TDS technique agree well with those determined by Hall measurement. Parameters for the complex dielectric function suitable for ITO in the range 0.2–2 and 4–450 THz are also determined.**

***Index Terms*— Dielectric function, drude free-electron model, indium tin oxide, optical constants, plasma frequency, scattering time, terahertz time domain spectroscopy.**

## I. Introduction

CONDUCTING indium tin oxide (ITO) is a wide-bandgap semiconductor that shows high optical transmission in the visible and near-infrared regions of the electromagnetic spectrum. ITO thin films are therefore widely employed as transparent electrodes for optoelectronic devices, such as solar cells, light emitting diodes, liquid crystal displays, etc. [1]–[3]. The wide range of potential applications of ITO films and related nanostructures has stimulated extensive studies of their preparation and characterization [3]–[20]. Numerous methods, such as evaporation, sputtering, chemical vapor deposition, pulsed laser deposition, and sol–gel processing, have been successfully employed for the deposition of ITO films on various substrates. Extensive works on the study of electrical and optical properties of ITO films have been reported [3]–[20]. The key material properties of ITO films for optoelectronic applications are low resistivity (<200 $\mu\Omega$ cm) and high transmittance (>90%) in the visible range.

It is interesting to explore the application of ITO films for the far-infrared, in view of the increasing use of terahertz (THz) devices for various applications, e.g., material characterization and identification, communications, imaging, medical diagnosis, health monitoring, environmental control, and chemical and biological sensing, as well as security and quality control applications [21]. In the past, the fixed and variable angle reflection and transmission Fourier transform infrared spectroscopy (FTIR) methods have been utilized to determine the electrical properties of the conducting coatings [3], [12]–[16]. Recently, THz time-domain spectroscopy (THz-TDS) has been employed to investigate the physical parameters of several materials, including bulk semiconductors [22], [23], thin metal films [24], epilayers, and nanostructures [25], [26]. To date, relatively few studies have been reported on the optical and electrical characteristics of ITO thin films in the THz frequency range [27], [28]. Bauer *et al.* [27] showed that ITO-coated glass could be used as dichroic mirrors for far-infrared radiation, while Jewell *et al.* [28] constructed a tunable Fabry–Perot etalon by sandwiching a liquid crystal between ITO-coated glasses. These earlier studies investigated commercially available ITO-coated glasses. It is well known that such borosilicate glass substrates absorb substantially at THz frequencies. Further, parameters for the dielectric response of ITO for a broad enough spectrum from the visible to the THz frequency range are not available. In this paper, we report the frequency-dependent complex THz conductivities and dielectric responses of several ITO thin films deposited on fused silica (FS) by THz-TDS. Using the Drude free-electron model, the key parameters that determine the free carrier dynamics of the ITO films are extracted. The electrical properties of the thin films derived from this noncontact optical technique agree well with those determined by FTIR reflectance spectroscopy and Hall measurements. The dependence of electrical properties of the ITO layer, such as carrier concentration and conductivity, on layer thickness is investigated and discussed

Manuscript received April 20, 2010; revised July 11, 2010; accepted July 25, 2010. Date of current version November 24, 2010. This work was supported by the National Science Council, Taiwan, under Grants NSC98-2120-M-006-003 and NSC96-2221-E-009-092-MY3.

C.-W. Chen, Y.-C. Lin, C.-H. Chang, and P. Yu are with the Department of Photonics and Institute of Electro-Optical Engineering, National Chiao Tung University, Hsinchu 30010, Taiwan (e-mail: cwchen.eo90g@nctu.edu.tw; choppy.eo96g@g2.nctu.edu.tw; nctueric.eo95g@nctu.edu.tw; yup@faculty.nctu.edu.tw).

J.-M. Shieh is with the Department of Photonics and Institute of Electro-Optical Engineering, National Chiao Tung University, Hsinchu 30010, Taiwan. He is also with the National Nano Devices Laboratories, Hsinchu 30078, Taiwan (e-mail: jmshieh@faculty.nctu.edu.tw).

C.-L. Pan is with the Department of Photonics and Institute of Electro-Optical Engineering, National Chiao Tung University, Hsinchu 30010, Taiwan. He is also with the Department of Physics and Institute of Photonics Technologies, National Tsing Hua University, Hsinchu 30013, Taiwan (e-mail: clpan@phys.nthu.edu.tw).

Color versions of one or more of the figures in this paper are available online at http://ieeexplore.ieee.org.

Digital Object Identifier 10.1109/JQE.2010.2063696

0018–9197/$26.00 © 2010 IEEE

in detail. This paper is organized as follows. In Section II, the experimental and theoretical methods are summarized. We then present and analyze experimental results in Section III. Finally, the main results are summarized in Section IV.

## II. Experimental and Theoretical Methods

### A. Preparation of the ITO Films

We have investigated several ITO thin films grown on FS substrates by dc reactive magnetron sputtering. The target was 8 in in diameter and composed of 95 wt.% $In_2O_3$ and 5 wt.% $SnO_2$. The sputter power was set at 300 W. During sputtering, argon (20 sccm) and oxygen (0.4 sccm) were introduced into the chamber and maintained at the total pressure of $6 \times 10^{-3}$ Torr. The substrates were kept at a fixed temperature of 250 °C. All the samples were as-grown thin films without post-deposition annealing. Film thicknesses of 189 $\pm$ 10, 483 $\pm$ 10, and 962 $\pm$ 10 nm were determined optically by use of an n&k Analyzer, model 1280. The carrier concentration and mobility of these samples were also determined by Hall measurements at room temperature (Ecopia HMS-3000).

### B. Determination of THz Optical Constants

A homemade antenna-based THz time-domain spectrometer with a collimated beam at the sample position was used [29]. A schematic of the THz-TDS experiment is shown in Fig. 1. THz-TDS measurements were performed at room temperature (300 K). The power spectral signal-to-noise ratio (SNR) is as high as $10^6$ (Fig. 2). Briefly, THz pulses generated from a femtosecond-laser-excited dipole-type antenna fabricated on low-temperature-grown GaAs were collimated by an off-axis paraboloidal mirror and propagated through the sample at normal incidence. The transmitted THz pulses were focused on another dipole-type antenna that was gated by time-delayed optical probe pulses and oriented to detect THz waves that were polarized parallel to the incident THz wave polarization. The diameter of the beam of the THz wave through each ITO sample was approximately 0.6 cm. The THz spectrometer was purged with nitrogen and maintained at a relative humidity of 3.0 $\pm$ 0.5%.

For extracting the optical constant, we consider the ITO layer (subscripted as 2) to be sandwiched between air (subscripted as 1) and a substrate (subscripted as 3) with refractive indices $n_2$, $n_1$, and $n_3$, respectively. The THz wave is assumed to be incident on this thin layer with a thickness of $d$ from the air toward the substrate. Taking into account multiple reflections [29], the transmitted THz electric field through the ITO-coated substrate can be written as

$$E_{sig}(\omega) = t_{31}E_0(\omega)\frac{t_{12}t_{23}e^{i\frac{n_2\omega d}{c}}}{1 - r_{21}r_{23}e^{i\frac{2n_2\omega d}{c}}}e^{i\frac{n_3\omega D}{c}} \quad (1)$$

where $E_0$, $t_{12}$, $t_{23}$, $t_{31}$, $r_{21}$, and $r_{23}$ are the incident electric field and transmission and reflection coefficients between various interfaces; $\omega$ is the angular frequency; $c$ is the speed of light in vacuum; and $D$ is the thickness of substrate. On the other hand, a reference THz field defined as the THz field transmitted through the bare substrate can be written as

$$E_{ref}(\omega) = t_{13}t_{31}E_0(\omega)e^{i\frac{\omega d + n_3\omega D}{c}}. \quad (2)$$

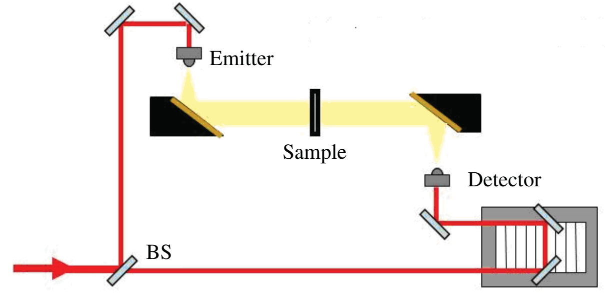


Fig. 1. General sketch of the homemade THz-TDS system. The arrow indicates laser pulses from a femtosecond Ti: sapphire laser; BS: optical beam splitter.

The transmittance of the THz wave through the ITO layer is then

$$t_{the}(\omega, n_2) = \frac{E_{sig}(\omega)}{E_{ref}(\omega)} = \frac{t_{12}t_{23}e^{i\frac{(n_2-1)\omega d}{c}}}{t_{13}\left(1 - r_{21}r_{23}e^{i\frac{2n_2\omega d}{c}}\right)}. \quad (3)$$

Experimentally, the transmittance $t_{\exp}(\omega, n_2)$ is obtained from ratios of the frequency components of the Fourier transforms of the measured THz waveforms through the ITO-coated sample and the bare substrate. An error function $Error(\omega, n_2)$ is defined as follows:

$$\left|t_{\exp}(\omega, n_2) - t_{the}(\omega, n_2)\right| = Error(\omega, n_2). \quad (4)$$

By minimizing the error function, the real and imaginary parts of the complex refractive index $n_2$ of the thin film layer can be deduced.

### C. Drude Free-Electron Model

In the Drude free-electron model, the dielectric function $\varepsilon(\omega)$ of a material, $\varepsilon(\omega) = [n(\omega) + ik(\omega)]^2$, consisting of contributions from bound electrons and conduction band electrons can be expressed as [30]

$$\varepsilon(\omega) = \varepsilon_\infty - \frac{\omega_P^2}{\omega^2 + \frac{i\omega}{\tau}}. \quad (5)$$

The first term on the right-hand side, i.e., $\varepsilon_\infty$, is the high-frequency dielectric constant contributed by valence electrons (bound electrons), while the second term arises from the free carriers for which $\tau$ is the momentum relaxation time. The characteristic plasma frequency $\omega_P$ is given by

$$\omega_P^2 = \frac{e^2 N_C}{m^* \varepsilon_0} \quad (6)$$

where $N_C$ is the concentration of free carriers, $m^*$ is the effective free-electron mass, and $e$ is the electron charge. The parameters $\omega_P$ and $\tau$ are obtained by best fitting of the measured dielectric constants. The mobility $\mu = e\tau/m^*$ can then be determined as well.

Now the dielectric function can be expressed as

$$\varepsilon(\omega) = N(\omega)^2 = (n(\omega) + ik(\omega))^2 = \varepsilon_\infty - \frac{\omega_P^2}{\omega^2 + \frac{i\omega}{\tau}} = \varepsilon_\infty + \frac{i\sigma}{\omega\varepsilon_0} \quad (7)$$

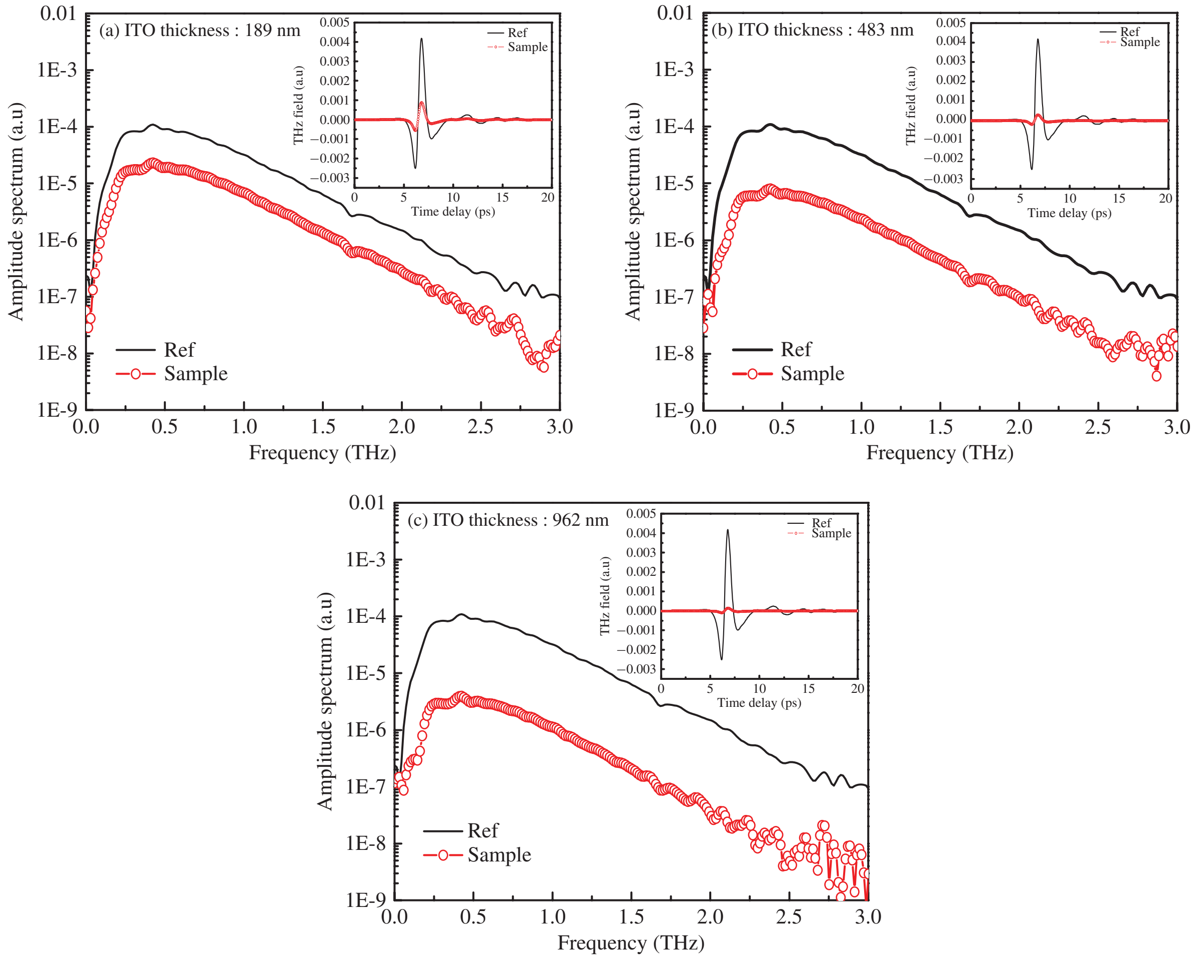


Fig. 2. Spectral and time profiles of the THz pulses transmitted through ITO films with thicknesses of (a) 189 nm, (b) 483 nm, and (c) 962 nm.

where $n(\omega)$ and $k(\omega)$ are the real and imaginary parts of the complex refraction index $N(\omega)$, respectively. In the Drude model, the complex conductivity is expressed as

$$\sigma(\omega) = \sigma_r(\omega) + i\sigma_i(\omega) = \frac{i\varepsilon_0\omega_P^2}{\omega + \frac{i}{\tau}} \tag{8}$$

where $\varepsilon_0 = 8.854 \times 10^{-12}$ (F/m) is the free-space permittivity. The real and imaginary parts of the conductivity $\sigma(\omega)$ are, respectively

$$\sigma_r(\omega) = 2nk\omega\varepsilon_0 \tag{9}$$

$$\sigma_i(\omega) = \varepsilon_0\omega\left(\varepsilon_\infty - n^2 + k^2\right) \tag{10}$$

where $\varepsilon_\infty = 4$ as given in [3]. From (8), the real and imaginary parts of $\sigma(\omega)$ can be rewritten as

$$\sigma_r(\omega) = \frac{\varepsilon_0\frac{\omega_P^2}{\tau}}{\omega^2 + \frac{1}{\tau^2}} \tag{11}$$

$$\sigma_i(\omega) = \frac{\varepsilon_0\omega\omega_P^2}{\omega^2 + \frac{1}{\tau^2}}. \tag{12}$$

### *D. FTIR Reflectance Spectroscopy*

The thickness of the ITO layer and the free charge carrier concentrations strongly affect its transmittance and reflectance spectra. At frequencies higher than $\omega_P$, transparent conducting oxide films such as ITO exhibit high transmittance. Conversely, they highly reflect the light for $\omega < \omega_P$ [3], [12]–[16]. A Bomen DA8.3 spectrometer was used to measure the specular power reflectance from the ITO sample surface with an oblique angle of incidence ($\theta \sim 18°$). We use the three-phase Fresnel equations of reflectance to model the ITO samples, which possess two dielectric interfaces. Here the three phases refer to a system consisting of air/ITO/substrate, where the FS is the substrate on which the ITO thin film is deposited. Here, the refractive index of air is assumed to have only a real component ($n = 1$, $k = 0$). The complex dielectric function of ITO follows the Drude free-electron model. As a first approximation, values for the complex refractive indices for FS over the spectral region from 4 to 450 THz are taken as $n = 1.4$, $k = 0$, which are the values of FS in the near-IR region. The three-phase model takes into account the decay in the magnitude of the electric field through the ITO and the refraction of the light through this layer before the radiation impinges on the ITO/FS interface. The general form of the ratio of the field amplitudes of reflected and incident radiation for a three-phase model of the Fresnel equation taking into account multiple reflections can be written as

$$r = \frac{r_{12} + r_{23}e^{2i\beta}}{1 + r_{12}r_{23}e^{2i\beta}} \tag{13}$$

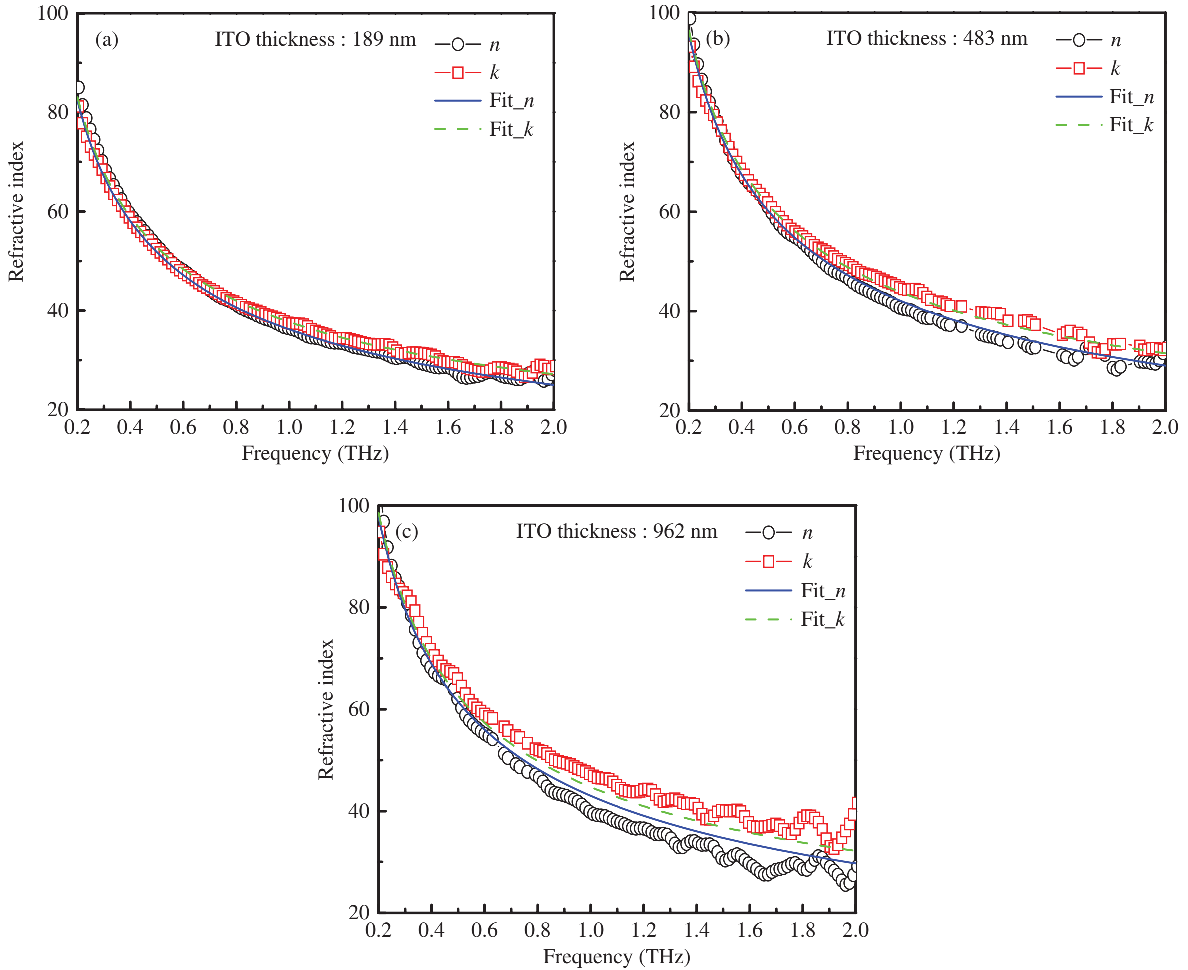


Fig. 3. Real (circles) and imaginary (squares) parts of the refractive index of the ITO thin film with thicknesses of (a) 189 nm, (b) 483 nm, and (c) 962 nm. Solid and dashed lines correspond to the calculated results based on the Drude free-electron model. The fitting parameters are listed in Table I.

where the various $r$'s on the right-hand side are the reflection coefficients at the various interfaces for p-polarization. The numeral subscripts (1, 2, 3) refer to the three phases (air, ITO, FS), respectively. The parameter $\beta$ is given by

$$\beta = 2\pi \left(\frac{d}{\lambda}\right) N_j \cos\theta_j \tag{14}$$

where $d$ is the thickness of the layer $j$, $\lambda$ is the wavelength of radiation, $N_j$ and $\theta$ are the complex refractive index of layer $j$ and the angle of the propagating beam relative to the surface normal in layer $j$, respectively. The general form of the Fresnel equations needed to determine $r_{12}$ and $r_{23}$ are

$$r_{jk} = \frac{N_j \cos\theta_j - N_k \cos\theta_k}{N_j \cos\theta_j + N_k \cos\theta_k} \tag{15}$$

where the subscripts $j$ and $k$ refer to the $j$th and $k$th phase of the model for layer $j$ (ITO) and layer $k$ (FS substrate), respectively. In (15), $\theta_k$ can be written as

$$\cos\theta_k = \sqrt{1 - \frac{\sin^2\theta_j}{N_k^2}} \tag{16}$$

where $\theta_k$ is the angle of the propagating wave in phase $k$ relative to the surface normal.

## III. Results and Discussions

In THz-TDS analysis, the measured time-domain THz waveforms from ITO thin films are first Fourier-transformed to obtain the power spectrum. The frequency-dependent dielectric constants of the samples are then calculated from the spectral amplitude and phase difference signals between those of the samples and the reference. In Fig. 2, we plot the measured THz spectra transmitted through the ITO samples of different thicknesses and of the reference. The corresponding THz time-domain waveforms are shown in the insets.

The real (circles) and imaginary (squares) parts of the THz refractive indices of the ITO thin films with different thicknesses are plotted in Fig. 3. The complex optical constants can be fitted quite well by the Drude free-electron model. Our results are in general agreement of previous reported values of Jewel *et al.* [28] up to 1.2 THz. Using (7) and (8), and with the high-frequency dielectric constant $\varepsilon_\infty$ for ITO thin film to be 4, we find that the real part of conductivity $\sigma_r(\omega)$ decreases slowly as the frequency increases, while imaginary part of conductivity, $\sigma_i(\omega)$ increases, as shown in Fig. 4. This frequency dependence is typical for Drude-like materials below the plasma frequency.

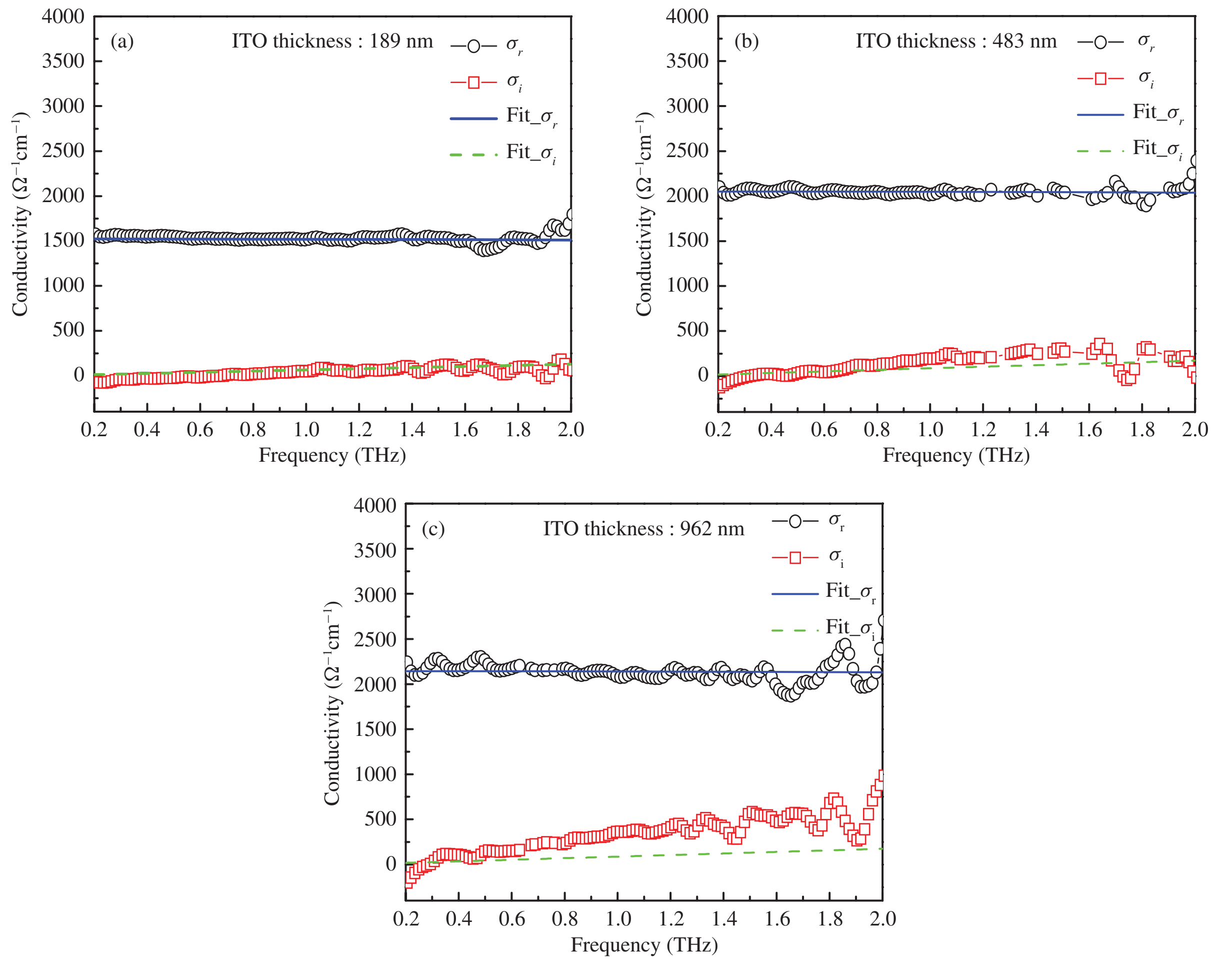


Fig. 4. Real (circles) and imaginary (squares) parts of conductivity of the ITO thin film with different thicknesses (a) 189 nm, (b) 483 nm, and (c) 962 nm. Solid and dashed lines correspond to the calculated results based on the Drude free-electron model. The fitting parameters are listed in Table I.

TABLE I

EXTRACTED PARAMETERS OF ITO THIN FILMS MEASURED BY THZ-TDS AND FTIR AND COMPARED TO THOSE OBTAINED FROM DC HALL MEASUREMENTS

| THz-TDS (nm) | $\omega_P$ (rad·THz) | $\tau$(fs) | $\mu$ (cm$^2$ V$^{-1}$ s$^{-1}$) | $n$ (cm$^{-3}$) | $\sigma$($\Omega^{-1}$cm$^{-1}$) |
|---|---|---|---|---|---|
| 189 | 1590 ± 10 | 6.8 ± 0.1 | 34.2 ± 0.5 | (2.79 ± 0.04) × $10^{20}$ | 1525 ± 44 |
| 483 | 1860 ± 10 | 6.7 ± 0.1 | 33.7 ± 0.5 | (3.81 ± 0.04) × $10^{20}$ | 2052 ± 52 |
| 962 | 1930 ± 20 | 6.5 ± 0.3 | 32.7 ± 1.5 | (4.10 ± 0.08) × $10^{20}$ | 2142 ± 142 |
| FTIR (nm) | $\omega_P$ (rad·THz) | $\tau$(fs) | $\mu$ (cm$^2$ V$^{-1}$ s$^{-1}$) | $n$ (cm$^{-3}$) | $\sigma$($\Omega^{-1}$cm$^{-1}$) |
| 189 | 1600 ± 15 | 6.9 ± 0.2 | 34.7 ± 1.0 | (2.82 ± 0.05) × $10^{20}$ | 1566 ± 73 |
| 483 | 1850 ± 10 | 6.6 ± 0.2 | 33.2 ± 1.0 | (3.77 ± 0.04) × $10^{20}$ | 2000 ± 82 |
| 962 | 1940 ± 10 | 5.8 ± 0.4 | 29.1 ± 2.0 | (4.14 ± 0.04) × $10^{20}$ | 1930 ± 153 |
| Hall (nm) | $\omega_P$ (rad·THz) | $\tau$(fs) | $\mu$ (cm$^2$ V$^{-1}$ s$^{-1}$) | $n$ (cm$^{-3}$) | $\sigma$($\Omega^{-1}$cm$^{-1}$) |
| 189 | | | 38.4 | 2.5 × $10^{20}$ | 1557 |
| 483 | | | 38.0 | 3.4 × $10^{20}$ | 2045 |
| 962 | | | 34.3 | 4.1 × $10^{20}$ | 2250 |

The dc conductivities for all samples are found to be in the range 1500–2200 $\Omega^{-1}$cm$^{-1}$. The parameters used for fitting the experimental data shown in Figs. 3 and 4, and the deduced electrical parameters for ITO are listed in Table I.

We find that the plasma frequency increases with the thickness of the ITO thin film. On the other hand, the electronic scattering time slightly decreased as the thickness of the ITO sample increased.

The value of the plasma frequency ($\omega_P$) is related to the charge carrier concentration ($N_C$) and the effective electron mass ($m^*$) of the ITO thin film as defined by the Drude free-electron model [see (6)]. Our data indicates that $\omega_P = 1590$

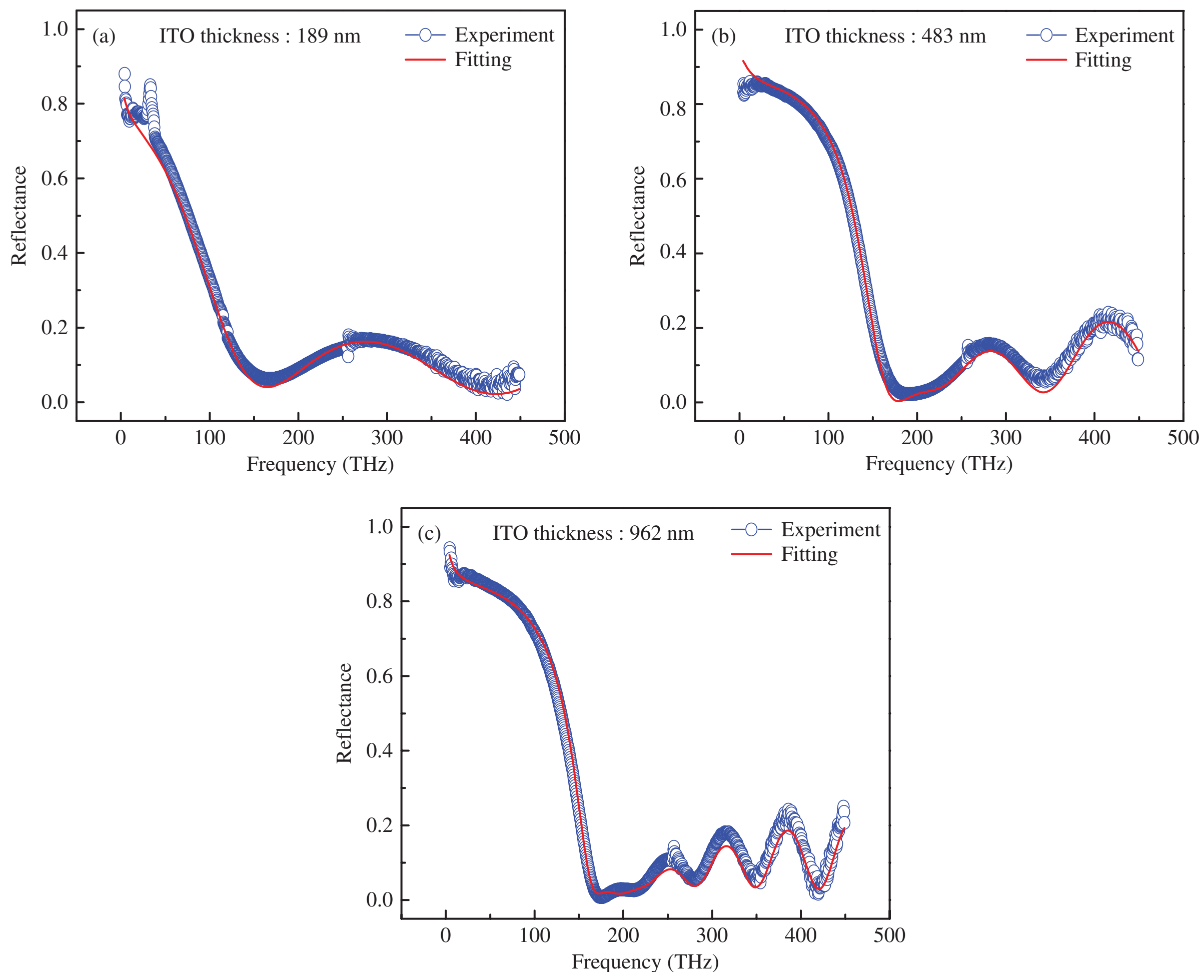


Fig. 5. Experimental (circles) and calculated (solid) FTIR p-polarized reflectance spectra for three ITO thin films with thickness of (a) 189 nm, (b) 483 nm, and (c) 962 nm.

$\pm$ 10 rad·THz and $\tau = 6.8 \pm 0.1$ fs for the 189-nm-thick ITO film; $\omega_P = 1860 \pm 10$ rad·THz and $\tau = 6.7 \pm 0.1$ fs for the 483-nm-thick sample; and $\omega_P = 1930 \pm 20$ rad·THz and $\tau = 6.5 \pm 0.3$ fs for the thickest sample investigated at 962 nm. Assuming an electron effective mass $m^* = 0.35m_0$ for the ITO thin film [3], these fitting parameters yield a carrier density $N_C = 2.79 \pm 0.04 \times 10^{20}$, $3.81 \pm 0.04 \times 10^{20}$, and $4.10 \pm 0.08 \times 10^{20}$ cm$^{-3}$ for 189-, 483-, and 962-nm-thick ITO films, respectively. The corresponding mobilities for these samples are 34.2 $\pm$ 0.5, 33.7 $\pm$ 0.5, and 32.7 $\pm$ 1.5 cm$^2$ V$^{-1}$ s$^{-1}$, respectively. The measured dielectric constants for thick sample in higher frequency show some deviations from those of the simulation results. It could possibly be caused by the low SNR in high-frequency region when a THz wave propagates through the thick sample. High SNR with broadband THz-TDS apparatus is desired for extraction of the wide-frequency-dependent dielectric constants. Therefore, different THz generation mechanisms, such as photoconductive switches, four-wave mixing, etc., lead the generated THz bandwidth from the narrow band to several tens THz.

By measuring the FTIR reflectance spectra of the ITO thin films, we have determined the positions of their plasma edges. Fig. 5 shows the experimental FTIR reflectance spectra including the region of the plasma frequency for ITO thin films of three different thicknesses recorded at an incident angle of 18° with p-polarized light. The calculated reflectance spectra obtained using the Drude free-electron model and the Fresnel equations for the three-layer (air/ITO/FS) structures are also shown. The fitted parameters for these ITO samples are listed in Table I. The value of the plasma frequency determines the spectral region of the observed sharp decrease in reflectance, while the electronic scattering time affects the curvature of the reflectance spectrum near the observed plasma frequency [3], [12]–[16]. The Drude free-electron model and the Fresnel equations of reflection accurately model the region of the reflectance spectra near the plasma frequency. In addition, the three-phase Fresnel equations of reflection accurately fit the experimental reflectance of the different ITO samples in the entire near-IR region studied. A gradual disappearance of the phonon-induced structure located around 10–40 THz for increasingly thick ITO layers is evident in Fig. 5. This is consistent with the observation that thinner conducting films, with lower carrier concentration, typically exhibit higher phonon strength. As summarized in Table I, carrier concentrations of the ITO layers, i.e., $N_C$, increase from $2.79 \times 10^{20}$ to $4.10 \times 10^{20}$ cm$^{-3}$ for increasingly thicker samples. The above picture is also in good agreement with those reported in the literature [3]. The oscillation for

frequencies larger than 200 THz is mainly due to the presence of the plasma frequency. Different location of the plasma frequency results in a completely different oscillation strength and profile.

For ease of analysis and avoiding the incorrect result, accurate measurement of the sample thickness is required. In this paper, we used the N&K analyzer to precisely verify the different thickness of the samples. Two parameters, i.e., plasma frequency and scattering time, are introduced in the fitting program to fit the wide-frequency-range FTIR data well. The oscillation data points and the whole curvature profile are necessary for accurate fitting. It is a fact that FTIR reflectance spectroscopy is a power tool to extract the information on plasma frequency located in the infrared range. However, THz-TDS provides another way not only to examine the optical constants in low frequency range but also to accurately obtain the electrical parameters such as plasma frequency and scattering time.

In Table I, a side-to-side comparison should convince us that the plasma frequencies and scattering times extracted from THz and optical reflectance spectra are in excellent agreements. Substituting the plasma frequency and scattering time into (7) allows us to write the dielectric function of ITO covering a broad spectral range of 0.2–450 THz. The THz- and FTIR-deduced values of electrical parameters, e.g., mobilities, carrier concentrations, and conductivities, are also in reasonable agreement with results of room-temperature Hall effect measurements. It is well known that Hall measurements can be affected by scattering from grain boundaries. On the contrary, the results derived from optical measurements are not affected by the grain sizes in the conducting films when the frequency is high enough [32]. For the samples investigated in this paper, the carrier mean free path in the ITO thin films is estimated to be less than 5 nm. This value is much smaller than the typical grain size (~100 nm) of the ITO thin film. Therefore, the optically and electrically determined carrier concentrations are close in our case. This result also agrees well with observations reported in the literature [33].

Previous workers have reported that the lattice distortion decreased with increasing film thickness for their sputtered ITO samples [9], [10]. This is physically reasonable because the larger the lattice distortion, the more oxygen interstitials are incorporated into the crystal lattice. Further, the microstrain in the samples would possibly also be larger. Consequently, the lattice distortion and the inhomogeneous microstrain decrease with increasing film thickness. Since the incorporated oxygen behaves as an electron trap, the carrier concentration increases with decreasing lattice distortion. This is consistent with our observations that the carrier concentration $N_C$ increases with increasing film thickness. In addition, Fig. 5 demonstrates clearly that reflectance increases with carrier concentration. This can be explained by the corresponding increase of the substitution Sn dopants [3].

The sputtering method is one of the most extensively used techniques for the deposition of ITO films. Table II summarizes the electrical properties of ITO films prepared by various groups using this technique [5]–[9]. Our data are also shown for comparison. Despite the difference in substrate temperature during the film-growth process and the post-deposition annealing temperature, even without the post-deposition heat treatment the mobilities of the sputtered ITO thin films all fall roughly in the range of 20–50 $cm^2\ V^{-1}\ s^{-1}$. The carrier concentrations are usually in the order of $10^{20}$–$10^{21}$ $cm^{-3}$. Consequently, the noncontact THz time-domain spectroscopic technique can be used confidently to determine dielectric and electrical properties of conducting thin films such as the ITOs. The characterization of nanostructured ITO coatings is under way in our laboratory. Such noncontact optical technique should give us a better understanding of the electrical parameters in nanostructured coatings.

TABLE II
ELECTRICAL PROPERTIES OF ITO FILMS PREPARED BY THE DC MAGNETRON SPUTTERING TECHNIQUE

| Thickness (nm) | $\mu$ ($cm^2\ V^{-1}\ s^{-1}$) | $n$ ($cm^{-3}$) | $\rho$ ($\Omega$cm) | References |
|---|---|---|---|---|
| 189 | 34.2 | $2.79 \times 10^{20}$ | $6.56 \times 10^{-4}$ | This paper |
| 483 | 33.7 | $3.81 \times 10^{20}$ | $4.87 \times 10^{-4}$ | This paper |
| 962 | 32.7 | $4.10 \times 10^{20}$ | $4.67 \times 10^{-4}$ | This paper |
| 301 | 47.5 | $10.7 \times 10^{20}$ | $1.23 \times 10^{-4}$ | [5] |
| 100 | 16.0 | $7.13 \times 10^{20}$ | $5.46 \times 10^{-4}$ | [6] |
| 300 | 24.5 | $7.0 \times 10^{20}$ | $3.7 \times 10^{-4}$ | [7] |
| 245 | 42.5 | $11.0 \times 10^{20}$ | $1.34 \times 10^{-4}$ | [8] |
| 270 | 48.7 | $8.5 \times 10^{20}$ | $1.51 \times 10^{-4}$ | [9] |
| 510 | 39.9 | $10.1 \times 10^{20}$ | $1.55 \times 10^{-4}$ | [9] |
| 960 | 42.7 | $9.9 \times 10^{20}$ | $1.48 \times 10^{-4}$ | [9] |

## IV. CONCLUSION

THz-TDS and FTIR reflectance spectroscopy were used to investigate the optical, dielectric, and electrical properties of ITO thin films. The data could be fitted satisfactorily by the Drude free-electron model. We have determined that the plasma frequencies of the ITO films are in the range of 1590–1930 rad·THz, while the corresponding scattering times are 6–7 fs for samples with three different thicknesses of 189, 483, and 962 nm. Such parameters allow the construction of the complex dielectric function for ITO thin films in the range of 0.2–2 and 4–450 THz. The mobilities and carrier concentration of the samples were determined to be 32.7–34.2 $cm^2\ V^{-1}\ s^{-1}$, and 2.79–4.10 $\times$ $10^{20}$ $cm^{-3}$, respectively. The electrical properties of the thin films derived from THz-TDS agree well with those determined by conventional Hall measurement and FTIR reflectance spectroscopy. Although it has been recently reported that the properties of ITO thin film are thickness-dependent [9], [10], a detailed study on the electrical and optical properties of ITO thin films from 189 to 962 nm thickness revealed only minor differences among them. The mobility and carrier concentration of nanostructured materials, which cannot be obtained easily by the typical Hall measurement, could thus be measured by such non-contact THz-TDS method.

## ACKNOWLEDGMENT

The authors would like to acknowledge technical support by the staff of the National Nano Devices Laboratories, Hsinchu, Taiwan.

## REFERENCES


[1] K. L. Chopra, S. Major, and D. K. Pandya, "Transparent conductors: A status review," *Thin Solid Films*, vol. 102, no. 1, pp. 1–46, Apr. 1983.

[2] C. G. Granqvist and A. Hultaker, "Transparent and conducting ITO films: New developments and applications," *Thin Solid Films*, vol. 411, no. 1, pp. 1–5, May 2002.

[3] I. Hamberg and C. G. Granqvist, "Evaporated Sn-doped $In_2O_3$ films: Basic optical properties and applications to energy-efficient windows," *J. Appl. Phys.*, vol. 60, no. 11, pp. R123–R160, Dec. 1986.

[4] R. B. H. Tahar, T. Ban, Y. Ohya, and Y. Takahashi, "Tin doped indium oxide thin films: Electrical properties," *J. Appl. Phys.*, vol. 83, no. 5, pp. 2631–2645, Mar. 1998.

[5] Y. Shigesato, S. Takaki, and T. Haranoh, "Electrical and structural properties of low resistivity tin-doped indium oxide films," *J. Appl. Phys.*, vol. 71, no. 7, pp. 3356–3364, Apr. 1992.

[6] S. Ishibashi, Y. Higuchi, Y. Ota, and K. Nakamura, "Low resistivity indium-tin oxide transparent conductive films. I. Effect of introducing $H_2O$ gas or $H_2$ gas during direct current magnetron sputtering," *J. Vac. Sci. Technol. A*, vol. 8, no. 3, pp. 1399–1402, May 1990.

[7] C. H. L. Weijtens, "Influence of deposition and anneal temperature on the electrical properties of indium tin oxide," *J. Electrochem. Soc.*, vol. 138, no. 11, pp. 3432–3434, 1991.

[8] H.-C. Lee and O. O. Park, "The evolution of the structural, electrical and optical properties in indium-tin-oxide thin film on glass substrate by DC reactive magnetron sputtering," *Vacuum*, vol. 80, no. 9, pp. 880–887, Jun. 2006.

[9] Z. Qiao, R. Latz, and D. Mergel, "Thickness dependence of $In_2O_3$:Sn film growth," *Thin Solid Films*, vol. 466, nos. 1–2, pp. 250–258, Nov. 2004.

[10] D. Mergel and Z. Qiao, "Correlation of lattice distortion with optical and electrical properties of $In_2O_3$ : Sn films," *J. Appl. Phys.*, vol. 95, no. 10, pp. 5608–5615, May 2004.

[11] J.-S. Cho, S.-K. Koh, and K. H. Yoon, "Microstructure and electrical properties of indium oxide thin films prepared by direct oxygen ion-assisted deposition," *J. Electrochem. Soc.*, vol. 147, no. 3, pp. 1065–1070, Mar. 2000.

[12] H. Kim, C. M. Gilmore, A. Pique, J. S. Horwitz, H. Mattoussi, H. Murata, Z. H. Kafafi, and D. B. Chrisey, "Electrical, optical, and structural properties of indium–tin–oxide thin films for organic light-emitting devices," *J. Appl. Phys.*, vol. 86, no. 11, pp. 6451–6461, 1999.

[13] P. K. Biswas, A. De, N. C. Pramanik, P. K. Chakraborty, K. Ortner, V. Hock, and S. Korder, "Effects of tin on IR reflectivity, thermal emissivity, Hall mobility and plasma wavelength of sol–gel indium tin oxide films on glass," *Mater. Lett.*, vol. 57, no. 15, pp. 2326–2332, Apr. 2003.

[14] S. H. Brewer and S. Franzen, "Indium tin oxide plasma frequency dependence on sheet resistance and surface adlayers determined by reflectance FTIR spectroscopy," *J. Phys. Chem. B*, vol. 106, no. 50, pp. 12986–12992, Nov. 2002.

[15] J. Ederth, G. A. Niklasson, A. Hultaker, P. Heszler, C. G. Granqvist, A. R. van Doorn, M. J. Jongerius, and D. Burgard, "Characterization of porous indium tin oxide thin films using effective medium theory," *J. Appl. Phys.*, vol. 93, no. 2, pp. 984–988, Jan. 2003.

[16] A. Solieman and M. A. Aegerter, "Modeling of optical and electrical properties of $In_2O_3$ : Sn coatings made by various techniques," *Thin Solid Films*, vol. 502, nos. 1–2, pp. 205–211, Apr. 2006.

[17] S. Takaki, Y. Aoshima, and R. Satoh, "Growth mechanism of indium tin oxide whiskers prepared by sputtering," *Jpn. J. Appl. Phys.*, vol. 46, no. 6A, pp. 3537–3544, 2007.

[18] Y. Yan, Y. Zhang, H. Zeng, J. Zhang, X. Cao, and L. Zhang, "Tunable synthesis of $In_2O_3$ nanowires, nanoarrows and nanorods," *Nanotechnol.*, vol. 18, no. 17, pp. 175601-1–175601-6, 2007.

[19] J. K. Kim, S. Chhajed, M. F. Schubert, E. F. Schubert, A. J. Fischer, M. H. Crawford, J. Cho, H. Kim, and C. Sone, "Light-extraction enhancement of GaInN light-emitting diodes by graded-refractive-index indium tin oxide anti-reflection contact," *Adv. Mater.*, vol. 20, no. 4, pp. 801–804, Jan. 2008.

[20] P. Yu, C.-H. Chang, C.-H. Chiu, C.-S. Yang, J.-C. Yu, H.-C. Kuo, S.-H. Hsu, and Y.-C. Chang, "Efficiency enhancement of GaAs photovoltaics employing antireflective indium tin oxide nanocolumns," *Adv. Mater.*, vol. 21, no. 16, pp. 1618–1621, Jan. 2009.

[21] X.-C. Zhang and J. Xu, *Introduction to THz Wave Photonics*. New York: Springer-Verlag, 2010.

[22] M. Hangyo, M. Tani, and T. Nagashima, "Terahertz time-domain spectroscopy of solids: A review," *Int. J. Infrared Millim. Waves*, vol. 26, no. 12, pp. 1661–1690, Dec. 2005.

[23] C.-W. Chen, T.-T. Tang, S.-H. Lin, J. Y. Huang, C.-S. Chang, P.-K. Chung, S.-T. Yen, and C.-L. Pan, "Optical properties and potential applications of $\varepsilon$-GaSe at terahertz frequencies," *J. Opt. Soc. Am. B*, vol. 26, no. 9, pp. A58–A65, 2009.

[24] N. Laman and D. Grischkowsky, "Terahertz conductivity of thin metal films," *Appl. Phys. Lett.*, vol. 93, no. 5, pp. 051105-1–051105-3, 2008.

[25] J. Han, Z. Zhu, S. Ray, A. K. Azad, W. Zhang, M. He, S. Li, and Y. Zhao, "Optical and dielectric properties of ZnO tetrapod structures at terahertz frequencies," *Appl. Phys. Lett.*, vol. 89, no. 3, pp. 031107-1–031107-3, Jul. 2006.

[26] H. Ahn, Y.-P. Ku, Y.-C. Wang, C.-H. Chuang, S. Gwo, and C.-L. Pan, "Terahertz spectroscopic study of vertically aligned InN nanorods," *Appl. Phys. Lett.*, vol. 91, no. 16, pp. 163105-1–163105-3, Oct. 2007.

[27] T. Bauer, J. S. Kolb, T. Löffler, E. Mohler, H. G. Roskos, and U. C. Pernisz, "Indium-tin-oxide-coated glass as dichroic mirror for far-infrared electromagnetic radiation," *J. Appl. Phys.*, vol. 92, no. 4, pp. 2210–2212, Aug. 2002.

[28] S. A. Jewell, E. Hendry, T. H. Isaac, and J. R. Sambles, "Tuneable Fabry–Perot etalon for terahertz radiation," *New J. Phys.*, vol. 10, no. 3, pp. 033012-1–033012-6, Mar. 2008.

[29] C.-L. Pan, C.-F. Hsieh, R.-P. Pan, M. Tanaka, F. Miyamaru, M. Tani, and M. Hangyo, "Control of enhanced THz transmission through metallic hole arrays using nematic liquid crystal," *Opt. Exp.*, vol. 13, no. 11, pp. 3921–3930, May 2005.

[30] M. Born and E. Wolf, *Principles of Optics: Electromagnetic Theory of Propagation, Interference and Diffraction of Light*, 7th ed. Cambridge, U.K.: Cambridge Univ. Press, 1999.

[31] F. Wooten, *Optical Properties of Solids*. San Diego, CA: Academic, 1972.

[32] J. Steinhauser, S. Fay, N. Oliveira, E. Vallat-Sauvain, and C. Ballif, "Transition between grain boundary and intragrain scattering transport mechanisms in boron-doped zinc oxide thin films," *Appl. Phys. Lett.*, vol. 90, no. 14, pp. 142107-1–142107-3, Apr. 2007.

[33] J. Hu and R. G. Gordon, "Textured aluminum-doped zinc oxide thin films from atmospheric pressure chemical-vapor deposition," *J. Appl. Phys.*, vol. 71, no. 2, pp. 880–890, Jan. 1992.

**Ching-Wei Chen** received the B.S. degree in physics from Tunghai University, Taichung City, Taiwan, the M.S. degree in engineering and system science from the National Tsing Hua University, Hsinchu, Taiwan, and the Ph.D. in electro-optical engineering from the National Chiao Tung University, Taiwain, in 2008.

He has been a Post-Doctoral Researcher in Prof. Ci-Ling Pan's group from 2008 to 2009. He joined as a Senior Engineer with the System Technology Division, LCD Panel Technology Department, AU Optronics Corporation, Hsinchu, in 2010.

His current research interests include ultrafast optics, terahertz photonics, optoelectronic materials, and photovoltaic technology.

**Yen-Cheng Lin** was born in Yunlin, Taiwan, in 1985. He received the B.S. degree in physics from the National Cheng Kung University, Tainan, Taiwan, and the M.S. degree in electro-optical engineering from the National Chiao Tung University, Hsinchu, Taiwan, in 2007 and 2009, respectively.

He is currently serving the one-year compulsory military duty in the army.

**Chia-Hua Chang** was born in Taipei, Taiwan, in 1983. He received the B.S. degree in materials science and engineering and the M.S. degree in electro-optical engineering from the National Chiao Tung University, Hsinchu, Taiwan, in 2006 and 2009, respectively. He is currently working toward the Ph.D. degree at the Institute of Electro-Optical Engineering, National Chiao Tung University.

His current research interests include the fabrication and simulation of indium-tin-oxide nanostructures on light-emitting devices and solar cell.

**Peichen Yu** (M'06) was born in Taipei, Taiwan, in 1974. She received the B.S. degree in electrophysics and the M.S. degree in electro-optical engineering from the National Chiao Tung University, Hsinchu, Taiwan, in 1996 and 1998, respectively. She received the Ph.D. degree in electrical engineering from the University of Michigan, Ann Arbor, in 2004.

She was a resolution enhancement techniques Design Engineer for the Advanced Design group of Intel Corporation, Hillsboro, OR, from 2004 to 2006. In 2006, she joined the Department of Photonics and the Institute of Electro-Optical Engineering at the National Chiao Tung University as an Assistant Professor and was promoted as an Associate Professor in August 2009. She is also actively engaged in the development of optical proximity correction and design for manufacturing solutions for complementary metal-oxide semiconductor 32 nm microlithography and beyond. Her current research interests include the design and development of nanostructured solar cells, light emitting diodes, and silicon-based nanodevices.

Dr. Yu is a member of the IEEE Photonics Society and the Society of Photographic Instrumentation Engineers.

**Jia-Min Shieh** received the Ph.D. degree in electro-optics from the National Chiao Tung University, Hsinchu, Taiwan, in 1997.

He is currently a Researcher with the National Nano Device Laboratories, Hsinchu, where he leads the photovoltaic/photonic device division. His academic interests include photovoltaic/photonic devices, and flexible electronics. His current research interests include developing efficient Si and CIGS thin-film solar cells embedded with various nanostructures and hybrid solar energy harvesting module and electronics/optoelectronics.

**Ci-Ling Pan** (M'88–SM'03) received the Ph.D. degree in physics from Colorado State University, Ft. Collins, in 1979.

He is currently Tsing Hua Chair Professor, Department of Physics and Institute of Photonics Technologies, Director of the Photonics Research Center, National Tsing Hua University (NTHU), Hsinchu, Taiwan. Prior to joining NTHU in February 2009, he was University Chair Professor, the Department of Photonics (DOP) and Institute of Electro-Optical Engineering (IEO), National Chiao Tung University (NCTU), Hsinchu. He served as the director of IEO, NCTU, from 1992 to 1995, and the founding Chair of the DOP from 2004 to 2006. He has also taken sabbatical leaves at the University of California, Berkeley, Osaka University, Osaka, Japan, and the Chinese University of Hong Kong, Hong Kong. His current research interests include lasers and their applications, e.g., material diagnostics, broadband optical communication, precision metrology, ultrafast, and THz Photonics.

Dr. Pan is a member of the Phi Tau Phi Honor Society in 1991, a Fellow of the Photonic Society of Chinese Americans in 1998, the Optical Society of America in 2004, the International Society of Optical Engineering in 2004, the Physical Society of Republic of China in 2005, and the American Physical Society in 2009. He was presented Merit Research Fellow Award of the National Science Council (NSC) in 2002, the Academics Award of the Ministry of Education in 2004, the Engineering Medal by the Optical Engineering Society, Taiwan, in 2004, Outstanding Engineering Professor Award of the Chinese Institute of Engineers in 2006, and the Pan Wen Yuan Foundation Research Excellence Award in 2007. The research outcome of his multi-universities project, "Photonic Science and Technology for the Tera-era," was selected as one of 50 across all disciplines in "Science 50," celebrating the 50th anniversary of NSC in 2008, and highlighted as the representative work for the field of optics and photonics in the 2008 NSC Science and Technology White Book.